International Journal of Minerals, Metallurgy and Materials
Volume 27, Number 1, January 2020, Page 63
https://doi.org/10.1007/s12613-019-1870-1

Hydrogen embrittlement of X80 pipeline steel in H_2S environment: Effect of hydrogen charging time, hydrogen-trapped state and hydrogen charging–releasing–recharging cycles

Peng-peng Bai[1,2], *Jie Zhou*[1,3], *Bing-wei Luo*[1], *Shu-qi Zheng*[1], *Peng-yan Wang*[4], *and Yu Tian*[2]

1) State Key Laboratory of Heavy Oil Processing, China University of Petroleum, Beijing 102249, China
2) State Key Laboratory of Tribology, Department of Mechanical Engineering, Tsinghua University, Beijing 100084, China
3) JAC Volkswagen Automotive Co., Ltd., Hefei 230601, China
4) SINOPEC Tenth Construction Company, Ltd., Qingdao 266555, China
(Received: 30 March 2019; revised: 28 May 2019; accepted: 3 June 2019)

Abstract: This study investigated the susceptibility of X80 pipeline steel to hydrogen embrittlement given different hydrogen pre-charging times and hydrogen charging–releasing–recharging cycles in H_2S environment. The fracture strain of the steel samples decreased with increasing hydrogen pre-charging time; this steel degradation could almost be recovered after diffusible hydrogen was removed when the hydrogen pre-charging time was <8 d. However, unrecoverable degeneration occurred when the hydrogen pre-charging time extended to 16–30 d. Moreover, nanovoid formation meant that the hydrogen damage to the steel under intermittent hydrogen pre-charging–releasing–recharging conditions was more serious than that under continuous hydrogen pre-charging conditions. This study illustrated that the mechanical degradation of steel is inevitable in an H_2S environment even if diffusible hydrogen is removed or visible hydrogen-induced cracking is neglected. Furthermore, the steel samples showed premature fractures and exhibited a hydrogen fatigue effect because the repeated entry and release of diffusible hydrogen promoted the formation of vacancies that aggregated into nanovoids. Our results provide valuable information on the mechanical degradation of steel in an H_2S environment, regarding the change rules of steel mechanical properties under different hydrogen pre-charging times and hydrogen charging–releasing–recharging cycles.

Keywords: high-strength steel; hydrogen embrittlement; corrosion; hydrogen diffusion

1. Introduction

Hydrogen typically enters into material during material preparation, processing, and servicing. Large mechanical devices such as ammonia units, hydrogenation reaction towers, industrial pipelines, and oil equipment function in a hydrogen environment [1–3]. Hydrogen sulfide (H_2S), a dangerous corrosive medium in sour oil or gas fields, can cause hydrogen-induced cracking, sulfide stress cracking, and stress- and hydrogen-induced cracking. These are generally considered to be hydrogen damage generated by corrosion processes and captured at hydrogen trapping [4–9]. Hydrogen embrittlement (HE) occurs when hydrogen dissolves into steel, and atomic hydrogen near the tips of cracks promotes their nucleation and propagation, ultimately resulting in mechanical degradation or even a steel fracture [10].

The main factors related to HE include hydrogen content and trapping state, dislocation development, vacancy formation, and material microstructure [11]. Takai *et al*. [12] found that HE susceptibility was high when hydrogen-induced lattice defects show a high formation trend and that vacancies play a primary role compared to hydrogen in hydrogen damage; this finding agrees well with the hydrogen-enhanced strain-induced vacancy model. Neeraj *et al*. [13] observed hydrogen-enhanced plastic flow localization and shear softening near the final fracture surface of steel, and proposed an alternative scenario in which plasticity-generated hydrogen-stabilized vacancy damage accumulation and de-

Corresponding authors: Shu-qi Zheng E-mail: zhengsq09@163.com; Yu Tian E-mail: tianyu@tsinghua.edu.cn

termined nanovoid coalescence was the failure pathway for HE. Xie *et al*. [14] found that vacancies generated by hydrogen play an important role in plastic flow localization in aluminum, which leads to hydrogen damage. Hattori *et al*. [15] observed the formation of hydrogen-enhanced strain-induced lattice defects before the formation of a final fracture in steel. Wan *et al*. [16] demonstrated that local activation caused a dislocation impingement/emission on the grain boundary and thus plays a key role in HE of metals. Momotani *et al*. [17] found that the elongation of hydrogen-charged low-carbon martensitic steel decreased significantly with decreasing strain rate. Pérez Escobar *et al*. [18] carried out thermal desorption spectroscopy (TDS) measurements and revealed that the microstructure of steel was more important than its carbon content in terms of hydrogen blister formation. Noh *et al*. [19] proposed that carbon enhances the planar slip and refines the mechanical twins, and found that an increased carbon content results in the formation of several hydrogen trapping and stress concentration sites, thereby accelerating HE.

In general, hydrogen in material can be divided into two categories: diffusible hydrogen and trapped hydrogen [20–21]. Diffusible hydrogen is captured by reversible hydrogen traps (such as dislocations, vacancies, and grain boundaries) and can be removed. Trapped hydrogen is captured by irreversible hydrogen traps (such as inclusions) and may be changed to diffusible hydrogen under certain conditions [22]. Not all hydrogen in a material can cause hydrogen damage to that material; a number of studies have shown that hydrogen damage is caused by diffusible hydrogen and that trapped hydrogen has no effect on material plasticity [23–25]. Moro *et al*. [26] found that hydrogen-induced decohesion along ferrite/pearlite interfaces and microcrack initiations on the external surface of X80 steel at high hydrogen pressure indicated that adsorbed and near-surface diffusible hydrogen were mainly responsible for HE. Zhu *et al*. [27] observed hydrogen-trapping sites directly using three-dimensional atom probe tomography and found that the solubility of hydrogen in austenite is more than three times that in martensite. Kim *et al*. [28] performed a stepwise hydrogen permeation experiment and suggested that hydrogen moves from the interstitial lattice to the irreversible trap site under certain stress levels.

The HE of pipeline steel in an H_2S environment is extremely dangerous because H_2S has a significantly higher adsorption capacity than H_2, leading to a higher hydrogen concentration (C_H) in steel under the former than under the latter. Therefore, hydrogen damage caused by wet H_2S has attracted considerable research attention. Huang *et al*. [29] found that transgranular propagation was the dominant mode of crack propagation in X80 steel in H_2S solution. Koyama *et al*. [30] revealed that low hydrogen content has no effect on the formation of fractures in, and the mechanical properties of Fe–Mn–C steel; however, the hydrogen damage became serious when the hydrogen content reached a certain level. Chen *et al*. [31] studied the influence of H_2S interaction on the mechanical properties of X80 steel with preexisting strains, and found that the elongation first decreased, and then increased, as the number of preexisting strains increased.

In previous studies, the operating conditions for steel in a hydrogen-related environment were kept constant and corrosion was found to be continuous. However, environmental media are constantly changing and in some cases, no corrosive media came into contact with the equipment. Diffusible hydrogen would rapidly escape steel after disengagement from the corrosive medium, which caused another scientific problem: the unclear mechanical properties of steel when hydrogen entry and escape occurs. Thus, this study examined the mechanical properties of steel samples pre-charged with hydrogen. Cyclic hydrogen charging–releasing–recharging tests were also carried out to investigate the effects of the hydrogen trapping state on HE. Hydrogen content in the samples was determined using Thermal Desorption Spectrometry (TDS). The morphology of the fracture surfaces was observed via scanning electron microscopy (SEM) and transmission electron microscopy (TEM).

2. Experimental

2.1. Materials

High-strength X80 pipe steel is widely used in long-distance transportation of oil and gas because of its satisfactory strength performance and low cost. However, the disadvantage of such high-strength, low-alloy steel is its hydrogen sensitivity [32]. This study used a piece of X80 steel in the form of a pipeline with a diameter of 1.2 m and thickness of 17 mm. The steel samples had the following chemical composition: 0.055wt% C, 1.3917wt% Mn, 0.2002wt% Si, 0.0019wt% S, 0.0017wt% P, 0.0318wt% Cr, 0.3184wt% Mo, 0.2636wt% Ni, and 0.0173wt% Al; the balance was Fe. X80 steel consists of ferrite, bainite, and acicular ferrite, as shown in Fig. 1.

2.2. Process

A flowchart of the hydrogen charging and tensile tests was shown by Fig. 2. The samples were annealed at 200°C

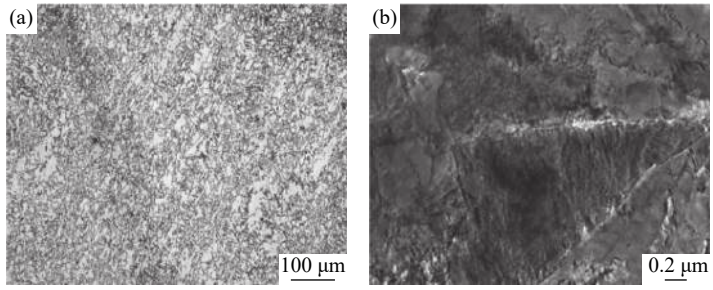

Fig. 1. Microstructure images of X80 steel by different analyses: (a) SEM; (b) bright-field TEM.

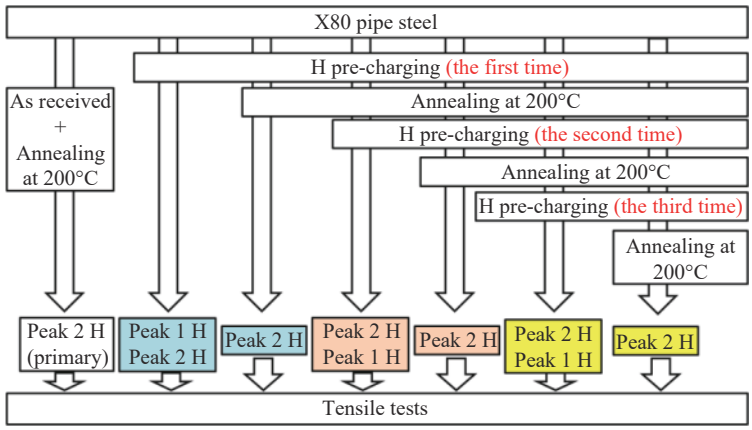

Fig. 2. Flow diagram of the charging and tensile tests used in this study. Peak 1 H and Peak 2 H represent the diffusible hydrogen and trapped hydrogen, respectively.

for 2 h to release diffusible hydrogen. Hydrogen was pre-charged into the steel samples by immersion in saturated H_2S NACE-A solution (5.0wt% NaCl + 0.5wt% CH_3COOH) for 2, 4, 8, 16, and 30 d (which are denoted "hydrogen pre-charging times"). Prior to the introduction of H_2S, the vessel containing the NACE-A solution and the samples was purged with N_2 for 1 h. an H_2S pressure of 0.1 MPa and the temperature of 25°C were maintained throughout the tests.

The hydrogen atom is present as both diffusible hydrogen (Peak 1 H) and trapped hydrogen (Peak 2 H) in the steel samples. Peak 1 H and Peak 2 H were achieved by the reversible and irreversible hydrogen traps, respectively. Diffusible hydrogen could always escape from the material at less than 200°C whereas trapped hydrogen needed the increased temperature to escape from the material. Thus, only trapped hydrogen existed in the sample after heat treatment at 200°C. This trapped hydrogen was used to study the effect of hydrogen trap states on the mechanical properties of X80 steel. Notably, the corrosion product film did not peel during any of the charging–releasing–recharging hydrogen tests. The hydrogen charging–annealing–recharging process was defined as the primary circulation test.

2.3. Tensile tests

The tensile tests had to be carried out quickly to avoid hydrogen diffusion while in progress. The tensile tests were conducted at a strain rate of 0.01 s^{-1} on a universal tensile testing machine with the temperature maintained at 25°C. The tensile sample diagram is shown in Fig. 3. The sample length after breakage, and the length and width of the fracture surface, were measured using a Vernier caliper to calculate the elongation of the sample.

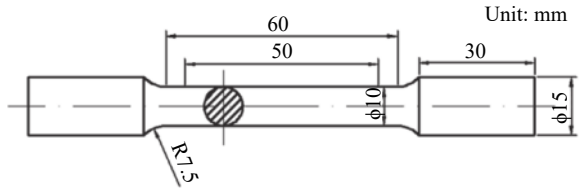

Fig. 3. Diagram of the sample for tensile tests.

2.4. Hydrogen concentration measurements

The hydrogen content in the sample was determined via TDS at a test speed of 100°C/h. This method has been used before in studies of the HE sensitivity of high-strength and ultrahigh-strength steels and other alloys [33], and has an analytical accuracy of up to 1.0×10^{-6}vol%; it can also simultaneously test the transient variations in hydrogen given changes in temperature.

2.5. Characterizations of fracture morphology

The morphology of the fracture surfaces was observed via SEM (FEI QUANTA 200F). However, many micromorphologies such as dislocations and vacancies cannot be observed by SEM. Therefore, a comprehensive TEM analysis was required to explain the intrinsic failure mechanism. TEM samples were prepared via electrolytic double-spraying using 5wt% perchloric acid–ethanol solution.

3. Results and discussion

3.1. Effect of hydrogen charging time on the mechanical properties of X80 steel

Fig. 4 illustrates the fracture behavior of X80 steel after hydrogen charging for 2, 4, 8, 16, and 30 d. As shown in the Fig. 4(a), the uncharged sample shows a distinct yield plateau while the pre-charged hydrogen samples do not show a yield stage at all. As the hydrogen charging time increased, the tensile and yield strength of steel increased slightly compared to those of the blank sample, in accordance with the theory that hardening occurs under a low-pressure hydrogen environment [34]. The blank sample was elongated by 19%, while that of the steel decreased significantly with increasing hydrogen charging time. This implies that the hydrogen damage to steel increases as hydrogen pre-charging time increases. Furthermore, the elongation of the steel decreased sharply for prolonged hydrogen pre-charging during the first 4 d, i.e., from 19% (uncharged) to 14.21% (after charging for 4 d). However, the change in elongation was small, being from 4 to 30 d; it decreased from 14.21% (charged for 4 d) to 12.83% (charged for 30 d). This outcome indicated that the range of plastic reduction decreased over that period. The main reasons for this phenomenon were the fact that hydrogen is not infinitely soluble in steel; there is a certain threshold value, at or near which the entry of hydrogen slows or the hydrogen content is balanced and escapes [35–36]. Kittel *et al*. [37] found that hydrogen-induced cracking under an H_2S environment will reach a stable state, depending mainly on pH and H_2S partial pressure. This finding is similar to our conclusion.

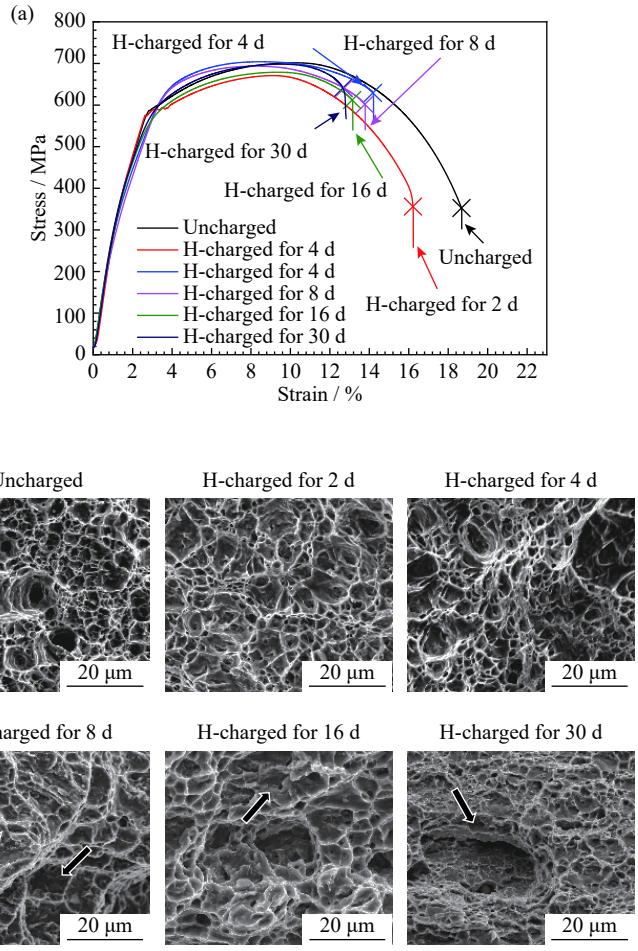

Fig. 4. Fracture behavior of X80 steel for different charging times: (a) stress–strain curves; (b) SEM images of the fracture surface.

Fig. 4(b) shows the SEM fractographs of the samples after the tensile tests. The fracture of the uncharged sample was elliptical and demonstrated distinct necking. The shearing lip was large and the fracture was fibrous at its center. These conditions indicated that the uncharged sample underwent ductile fracturing; the fibrous area was composed mainly of many large and deeply equiaxed dimples. The SEM fractographs of the samples after hydrogen charging for 2–30 d show that the tensile fracture was relatively flat and that the shear lip was very small. As the hydrogen charging time increased, the fracture gradually changed from ductile to a combination of ductile and quasi-cleavage types. In addition, the dimples became small and shallow. The quasi-cleavage fracture became more pronounced with the increase in hydrogen charging time, as indicated by the black arrow.

3.2. Recovery of mechanical properties of X80 steel after hydrogen discharge

Fig. 5 compares the mechanical properties of uncharged, hydrogen pre-charged, and hydrogen-released steel by heat treatment (HT) at 200°C. Figs. 5(a)–5(d) illustrate the changes in the stress–strain curves. The black, blue, and red lines represent the hydrogen-uncharged, hydrogen pre-

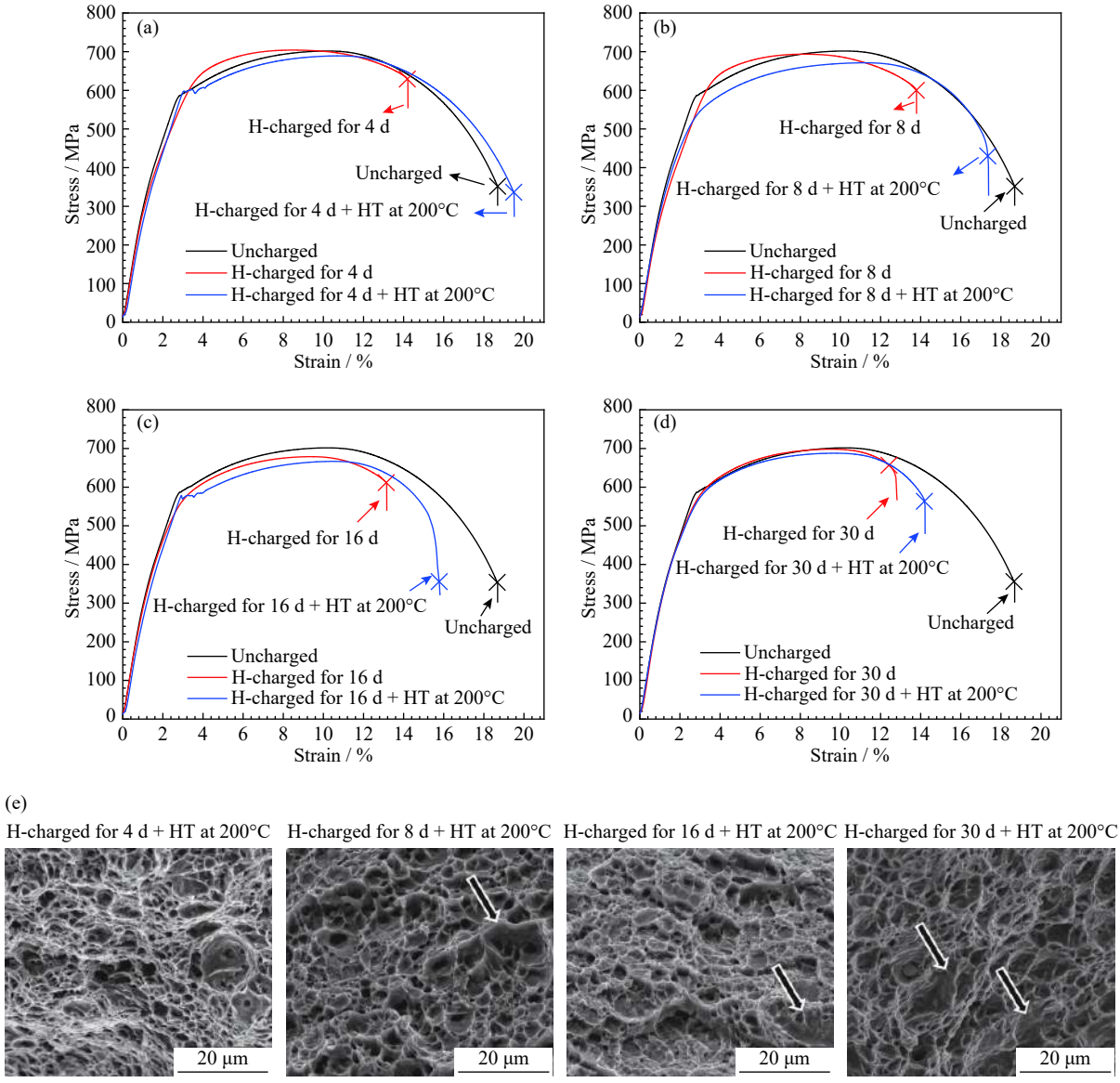

Fig. 5. Mechanical properties of X80 steel after releasing the charged hydrogen: (a–d) comparison of the mechanical properties before and after hydrogen release for different hydrogen charging processes; (e) SEM fracture morphologies of hydrogen pre-charged steel after hydrogen release.

charged, and hydrogen-released samples, respectively. In the samples pre-charged for 4 and 8 d (Figs. 5(a)–5(b)), the elongation after hydrogen release almost reverted to the level of the uncharged sample. In addition, the tensile strength and yield strength exhibited no distinct changes, indicating that the damage caused by hydrogen is reversible and can be recovered by releasing hydrogen. Meanwhile, only annealing promoted the escape of the diffused hydrogen but had no effect on trapped hydrogen. Hence, the trapped hydrogen was retained in the steel after annealing, indicating that it had no effect on the mechanical properties of the steel. However, in the samples pre-charged with hydrogen for 16 and 30 d (Figs. 5(c)–(d)), the elongation of samples after hydrogen release could not revert to the level of uncharged sample. This indicates that irreversible damage had occurred after immersion in the H_2S solution, despite the release of the diffusible hydrogen. Irreversible damage in the form of micro-cracks and hydrogen bubbles was caused by hydrogen when the hydrogen concentration in the steel was higher than the critical hydrogen concentration. Once defects were formed, the plasticity of the steel could not recover, resulting in early rupture; moreover, hydrogen blister rupture would generate many micro-cracks [38]. Remarkably, hydrogen cracking and hydrogen bubbling were not observed in our study, as supported by the following reason for the failure to recover. Comparing the blue curves in Figs. 5(c) and 5(d), the irreversible hydrogen damage of the samples after hydrogen pre-charging for 30 d was more serious than that after hydrogen pre-charging for 16 d. This indicated that the performance degradation of the steel under H_2S solution was inevitable, even if diffusible hydrogen had been released.

Fig. 5(e) shows the fracture morphologies of the hydrogen-released samples after the tensile tests; the necking at fracture is clearly observed. This outcome was very different from that presented in Fig. 4(b). In addition, the necking section gradually weakened with increasing hydrogen pre-charging time, and the shrinkage of the section decreased gradually. These observations also proved that the irreversible hydrogen damage of steel becomes severe with increasing hydrogen pre-charging time. For the sample pre-charged with hydrogen for 4 d, the plastic fracture characteristics were most pronounced after annealing. In addition, many dimples could be seen, indicating that the steel plastic had recovered after hydrogen escaped. However, for the samples pre-charged with hydrogen for 8–30 d, apart from dimples, several tear edges and step patterns could be seen on the fracture surface. This indicated that the steel was damaged by hydrogen, although the plasticity was restored to a certain extent.

3.3. Mechanical properties of X80 steel undergoing hydrogen charging and releasing circulation tests

The results in the previous section showed that steel elongation decreased with increasing pre-charging time; however, this decrease was not continuous because the amount of diffusible hydrogen in the material had a certain threshold. In addition, the mechanical properties of steel could be restored by releasing the diffusible hydrogen for a pre-charging duration of less than 8 d. This would imply that the tensile properties of the steel could be restored by timely removal of the diffusible hydrogen from the material. This result needs to be elucidated.

The tensile test results shown in Fig. 6 indicate an elongation of 19% for the uncharged sample. Fig. 6(a) shows that the elongation of steel reduced to 14.2% after hydrogen pre-charging for 4 d, recovered to 19.7% after annealing, and then sharply decreased to 11.1% after hydrogen recharging for 4 d. This elongation was lower than that of the sample immersed for 30 d. Meanwhile, the tensile strength distinctly decreased to 627 MPa. Fig. 6(b) illustrates that the steel elongation decreased to 16.2% after hydrogen pre-charging for 2 d and to 13.8% after 2 cycles of hydrogen charging/discharging. Meanwhile, the tensile strength decreased slightly. Fig. 6(c) shows that the steel elongation decreased to 16.2% after hydrogen pre-charging for 2 d and to 13.9% after three cycles of hydrogen charging/discharging; the tensile strength decreased slightly. In contrast to the blue line in Figs. 6(b) and 6(c), the elongations of the samples subjected to two and three cycles of hydrogen charging/discharging were almost the same despite the total hydrogen charging time being shorter for the former than the latter, as shown in Fig. 6(c). This indicated that a threshold exists for steel, which is formed by hydrogen at a hydrogen charging time of two d. Furthermore, greater hydrogen damage was not caused when the hydrogen in the steel was close to or reached the threshold. In Figs. 6(a)–6(c), the elongation of steel represented by the blue line was much lower than that represented by the red line, despite the last time duration of hydrogen charging being the same. The results indicated that steel was fatigued with hydrogen. However, this phenomenon needs to be clearly confirmed.

Figs. 6(d)–6(f) show the SEM images of the fracture surfaces related to the blue line in Figs. 6(a)–6(c). The fracture mode of all samples was cleavage fracture, with no dimples. In addition, many secondary cracks were observed on the cross-section, as well as on some tearing edges. These findings indicated the occurrence of almost no plastic deformation, but completely brittle fracture.

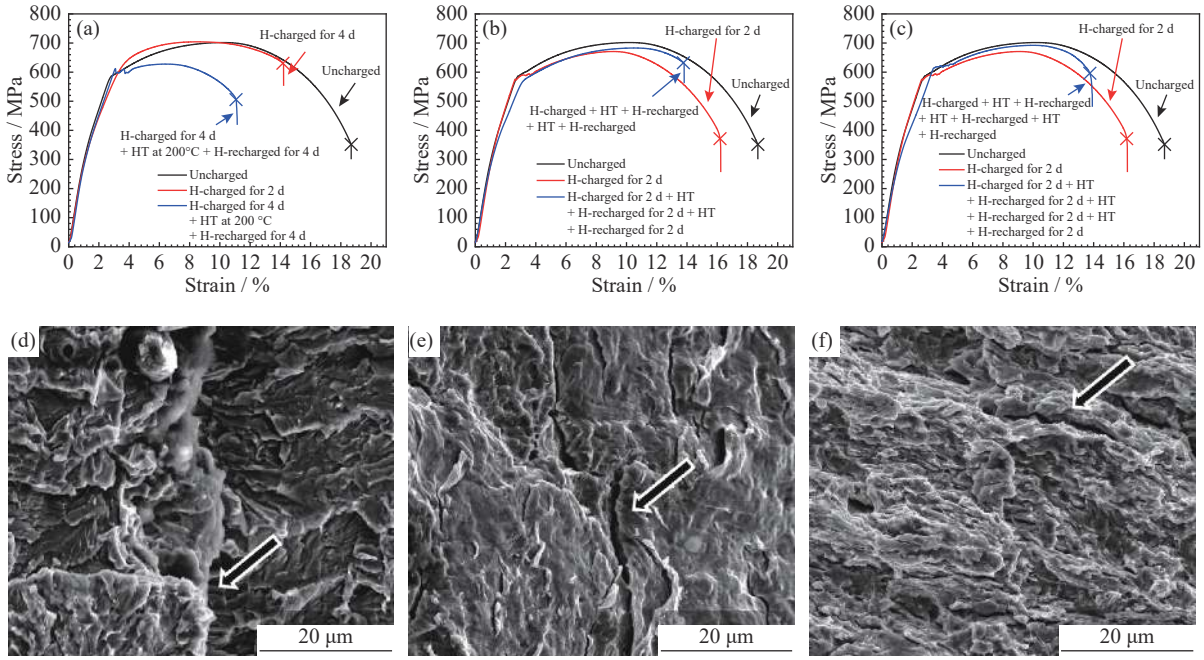

Fig. 6. Mechanical properties of X80 steel after the circulation test of hydrogen pre-charging and release: (a) 1 cycle of hydrogen charging/discharging process; (b) 2 cycles of hydrogen charging/discharging process; (c) 3 cycles of hydrogen charging/discharging process; (d–f) morphologies of the fracture surfaces corresponding to the blue lines in (a), (b), and (c), respectively.

3.4. Hydrogen content and nano characteristics of steel under different hydrogen pre-charging conditions

Fig. 7(a) shows the hydrogen content of samples under different hydrogen charging processes. Under the heating rate of 100°C/h, the diffusible hydrogen of the uncharged sample was approximately 3.22×10^{-10}vol%. The diffusible hydrogen contents of the samples with hydrogen pre-charging for 4 d and 8 d were 1.37×10^{-4}vol% and 1.63×10^{-4}vol%, respectively. The diffusible hydrogen in steel increased by approximately 0.26×10^{-4}vol% when the immersion time extended from 4 d to 8 d. The diffusible hydrogen of the hydrogen-recharged sample at 4 d after hydrogen charging 4 d, followed by annealing, was 1.81×10^{-4}vol%, and increased by 0.44×10^{-6}vol% compared with that of steel after 4 d of immersion. In contrast to the hydrogen above 200°C, the trapped hydrogen in steel increased by approximately 0.25×10^{-4}vol% when the immersion time extended from 4 d to 8 d. The trapped hydrogen in steel, hydrogen-recharged at 4 d following hydrogen charging for 4 d followed by annealing, was 0.11×10^{-4}vol%, and increased by 0.03×10^{-4}vol% compared with that of steel after 4 d of immersion. The total hydrogen content in the sample immersed for 4 d was least, but increased with prolonged immersion time. The total hydrogen content in the sample under the 1 cycle hydrogen charging and releasing process hydrogen charging and releasing was similar to that in the sample immersed for 8 d.

The advantage of TDS analysis is that the type of hydrogen trap can be determined from the temperature of hydrogen escape [39]. Fig. 7(b) shows the diffusion rate of hydrogen with increasing temperature. All four curves have a small peak at approximately 395°C. The blue curve represents the blank sample without change in hydrogen content. It indicates that this part of the hydrogen was the original hydrogen content in steel, which existed as trapped hydrogen, and mainly arose due to the diffusion of hydrogen atoms into the metal during steel pickling [40]. The samples immersed for 4 d exhibited two peaks at approximately 96 and 395°C, which could be identified as the escape positions of diffusible hydrogen and trapped hydrogen, respectively. The peaks at approximately 96°C could be attributed to hydrogen escape from grain boundaries and dislocations. The peaks at approximately 395°C could be attributed to hydrogen escape from inclusions. The samples immersed for 8 d exhibited peaks at 102, 205, 278, 298, and 395°C. Peaks at 102 and 395°C were also exhibited by the sample immersed for 4 d. The peaks at 205, 278, and 298°C may correspond to the hydrogen escape from vacancies, indicating that hydrogen migrated from the dislocation and grain boundary to vacancies with increasing immersion time. This finding is consistent with the hydrogen-induced vacancy theory [41–42]. The steel subjected to hydrogen recharging at 4 d after hydrogen charging for that period, followed by annealing, was similar to the sample

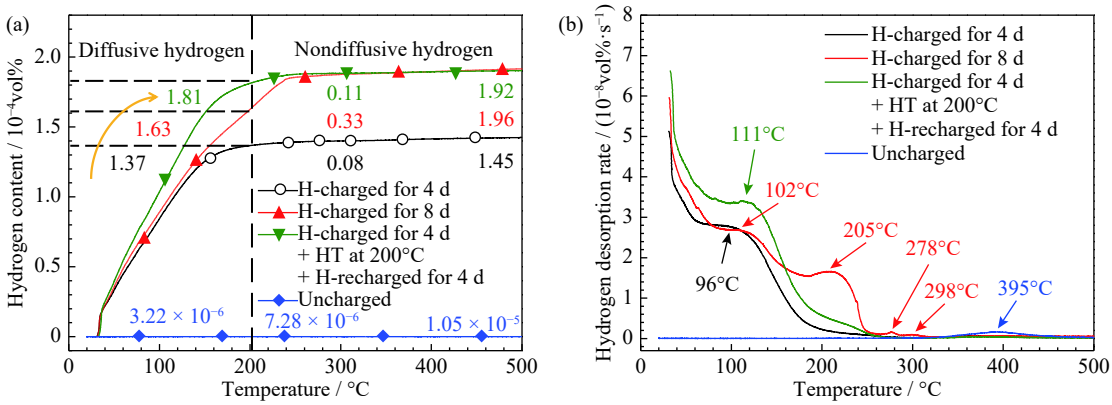

Fig. 7. Hydrogen content (a) and typical hydrogen desorption curves (b) of the samples for different hydrogen charging processes.

immersed for 4 d. Two peaks were observed at 111 and 395°C, which could be regarded as the trapped locations of diffusible hydrogen and trapped hydrogen, respectively. Compared with the samples hydrogen pre-charged for 4 and 8 d, the diffusible hydrogen peak shifted to the right by approximately 10°. This phenomenon may have been due to the increased number of hydrogen trapping sites, in addition to grain boundary and dislocation sites, such as nanovoids. The above results showed that hydrogen diffuses from the low-binding energy level to the high-binding-energy level in steel with increasing immersion time for hydrogen pre-charging. In addition, several hydrogen trapping sites emerged with increasing time for hydrogen pre-charging. Hydrogen recharging also seriously affected the amount of diffused hydrogen in steel. Some diffuse hydrogen trapping sites were formed and caused a peak shift of diffusible hydrogen by 10° to the right side. The diffusible hydrogen content increased on recharge after hydrogen discharge, which was the main reason for the decrease in elongation.

Fig. 8 shows the TEM images of the steel fracture area after tensile tests. For the blank tensile samples without hydrogen pre-charging, the grain boundary was clear, and the grains exhibited distinct elongation. Nevertheless, no dislocation was observed in the grains, and only a few dislocations were found at the grain boundaries, as shown in Figs. 8(a)–8(c) show the steel microstructure after 4 and 8 d of hydrogen pre-charging; the grain was markedly elongated. Several clutter dislocations twisted into a bundle were mainly

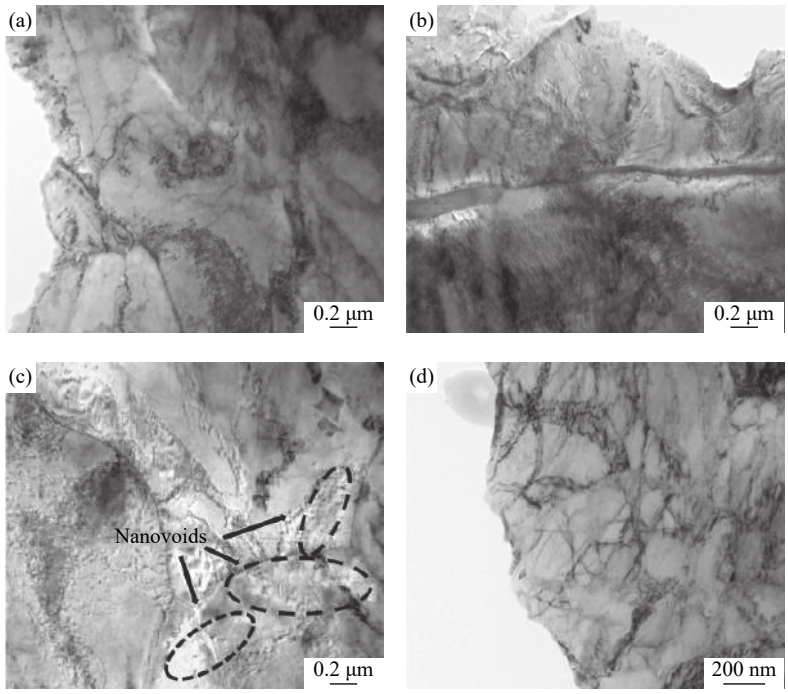

Fig. 8. Bright-field TEM images of the fracture area of steel samples after tensile test for different hydrogen charging processes: (a) uncharged; (b) H-charged for 4 d; (c) H-charged for 4 d + HT + H-recharged for 4 d; (d) H-charged for 8 d.

concentrated in the vicinity of the grain boundaries. The main reason for this behavior was that plastic deformation produced a large number of dislocations, and the occurrence of hydrogen-reduced dislocation nucleation could promote dislocation [43]. At the same time, hydrogen could be easily captured in combination with dislocation because dislocation corresponds to reversible hydrogen trapping. The existence of hydrogen reduced the migration performance, thereby causing dislocation accumulation and reducing the steel plasticity.

Fig. 8(d) shows the steel hydrogen-recharged for 4 d after hydrogen charging (4 d) followed by annealing. Dislocations, which were more than those in the blank sample, were clearly observed. Nevertheless, the dislocation density was significantly lower than that of the sample hydrogen pre-charged for 4 d. However, some nanovoids were visible in the white ellipse, with size <100 nm. The decrease in the dislocation density and increase in nanovoids indicated that the theory of interaction between hydrogen and dislocation is no longer applicable for this situation. However, the theory of interaction between hydrogen and a vacancy might be applicable [44], and is explained as follows: the material at the crack tip deformed and showed dislocation plasticity; a local plastic zone also formed at the regions with increased local hydrogen content produced by hydrogen accumulation; the aided local deformation zone had a high plasticity, generating excess vacancies [45–46]. Hydrogen combined with vacancies to form a hydrogen vacancy bond [45]. Therefore, a large number of vacancies gathered due to hydrogen accumulation. This phenomenon caused the nanovoids to nucleate and grow, resulting in the ultimate material fracture.

4. Conclusions

(1) With the extension of hydrogen pre-charging time, hydrogen damage becomes increasingly severe but eventually reaches a stable state. A hybrid tensile fracture forms with the extension of hydrogen pre-charging time, i.e., it gradually transforms from ductile fracture into ductile fracture and quasi-cleavage fracture, and finally transforms into complete quasi-cleavage fracture. The degree of deterioration of the mechanical properties of the samples decreased after continuous hydrogen pre-charging for 8 d.

(2) After annealing at 200°C, steel degradation almost recovers due to the removal of diffusible hydrogen when the hydrogen pre-charging time is less than 8 d. When the hydrogen pre-charging time is more than 8 d, the mechanical properties of steel cannot be restored despite the released diffusible hydrogen. This result indicated that irreversible damage occurred; nevertheless, hydrogen bubbling and hydrogen-induced cracking were not detected in all samples.

(3) For the samples under continuous hydrogen pre-charging, the main reason for fracture was the combination of hydrogen with dislocations, and a pinning dislocation effect. Subsequently, the dislocation slip was blocked, thereby finally reducing the material plasticity. For the samples under intermittent hydrogen pre-charging, dislocation plasticity produced vacancies and aggregated into nanovoids, leading to nanovoid nucleation and growth, and finally causing the fracture of materials.

Acknowledgements

This work was financially supported by the National Natural Science Foundation of China (Nos. 51805292, 51671215, and 51425502) and the National Postdoctoral Program for Innovative Talents of China (No. BX201700132).

References

[1] M.R. Louthan Jr, G.R. Caskey Jr, J.A. Donovan, and D.E. Rawl Jr, Hydrogen embrittlement of metals, *Mater. Sci. Eng.*, 10(1972), p. 357.

[2] P.P. Bai, J. Zhou, B.W. Luo, S.Q. Zheng, and C.F. Chen, Roles of carbon dioxide and steam on the hydrogen embrittlement of 3Cr tube steel in synthetic natural gas environment, *Corros. Eng. Sci. Technol.*, 53(2018), No. 1, p. 1.

[3] M. Koyama, E. Akiyama, Y.K. Lee, D. Raabe, and K. Tsuzaki, Overview of hydrogen embrittlement in high-Mn steels, *Int. J. Hydrogen Energy*, 42(2017), No. 17, p. 12706.

[4] A. Kawashima, K. Hashimoto, and S. Shimodaira, Hydrogen electrode reaction and hydrogen embrittlement of mild steel in hydrogen sulfide solutions, *Corrosion*, 32(1976), No. 8, p. 321.

[5] B.J. Berkowitz and H.H. Horowitz, The role of H_2S in the corrosion and hydrogen embrittlement of steel, *J. Electrochem. Soc.*, 129(1982), No. 3, p. 468.

[6] J. Woodtli and R. Kieselbach, Damage due to hydrogen embrittlement and stress corrosion cracking, *Eng. Fail. Anal.*, 7(2000), No. 6, p. 427.

[7] F.D. de Moraes, F.L. Bastian, and J.A. Ponciano, Influence of dynamic straining on hydrogen embrittlement of UNS-G41300 and UNS-S31803 steels in a low H_2S concentration environment, *Corros. Sci.*, 47(2005), No. 6, p. 1325.

[8] M. Monnot, R.P. Nogueira, V. Roche, G. Berthomé, E. Chauveau, R. Estevez, and M. Mantel, Sulfide stress corrosion study of a super martensitic stainless steel in H_2S sour environments: Metallic sulfides formation and hydrogen embrittlement, *Appl. Surf. Sci.*, 394(2017), p. 132.

[9] S.H. Li, C.F. Chen, Y.N. Liu, H.B. Yu, and X.L. Wang, Influence of surface martensite layer on hydrogen embrittle-

ment of Fe–Mn–C–Mo steels in wet H_2S environment, *Int. J. Hydrogen Energy*, 43(2018), No. 34, p. 16728.
[10] W.Y. Chu, L.J. Qiao, Q.Z. Chen, and K.W. Gao, *Fracture and Environment Induced Cracking*, Sciences Express, Beijing, 2000, p. 106.
[11] J.P. Hirth, Effects of hydrogen on the properties of iron and steel, *Metall. Trans. A*, 11(1980), No. 6, p. 861.
[12] K. Takai, H. Shoda, H. Suzuki, and M. Nagumo, Lattice defects dominating hydrogen-related failure of metals, *Acta Mater.*, 56(2008), No. 18, p. 5158.
[13] T. Neeraj, R. Srinivasan, and J. Li, Hydrogen embrittlement of ferritic steels: observations on deformation microstructure, nanoscale dimples and failure by nanovoiding, *Acta Mater.*, 60(2012), No. 13-14, p. 5160.
[14] D.G. Xie, S.Z. Li, M. Li, Z.J. Wang, P. Gumbsch, J. Sun, E. Ma, and Z. Shan, Hydrogenated vacancies lock dislocations in aluminium, *Nat. Commun.*, 7(2016), art. No. 13341.
[15] M. Hattori, H. Suzuki, Y. Seko, and K. Takai, The role of hydrogen-enhanced strain-induced lattice defects on hydrogen embrittlement susceptibility of X80 pipeline steel, *JOM*, 69(2017), No. 8, p. 1375.
[16] L. Wan, W.T. Geng, A. Ishii, J.P. Du, Q.S. Mei, N. Ishikawa, H. Kimizuka, and S. Ogata, Hydrogen embrittlement controlled by reaction of dislocation with grain boundary in alpha-iron, *Int. J. Plast.*, 112(2019), p. 206.
[17] Y. Momotani, A. Shibata, D. Terada, and N. Tsuji, Effect of strain rate on hydrogen embrittlement in low-carbon martensitic steel, *Int. J. Hydrogen Energy*, 42(2017), No. 5, p. 3371.
[18] D. Pérez Escobar, T. Depover, E. Wallaert, L. Duprez, M. Verhaege, and K. Verbeken, Thermal desorption spectroscopy study of the interaction between hydrogen and different microstructural constituents in lab cast Fe–C alloys, *Corros. Sci.*, 65(2012), p. 199.
[19] H.S. Noh, J.H. Kang, K.M. Kim, and S.J. Kim, The effect of carbon on hydrogen embrittlement in stable Cr–Ni–Mn–N austenitic stainless steels, *Corros. Sci.*, 124(2017), p. 63.
[20] R.A. Oriani, The diffusion and trapping of hydrogen in steel, *Acta Metall.*, 18(1970), No. 1, p. 147.
[21] M.Q. Wang, E. Akiyama, and K. Tsuzaki, Effect of hydrogen on the fracture behavior of high strength steel during slow strain rate test, *Corros. Sci.*, 49(2007), No. 11, p. 4081.
[22] W.K. Kim, S.U. Koh, B.Y. Yang, and K.Y. Kim, Effect of environmental and metallurgical factors on hydrogen induced cracking of HSLA steels, *Corros. Sci.*, 50(2008), No. 12, p. 3336.
[23] K. Takai and R. Watanuki, Hydrogen in trapping states innocuous to environmental degradation of high-strength steels, *ISIJ Int.*, 43(2003), No. 4, p. 520.
[24] M. Koyama, C.C. Tasan, E. Akiyama, K. Tsuzaki, and D. Raabe, Hydrogen-assisted decohesion and localized plasticity in dual-phase steel, *Acta Mater.*, 70(2014), p. 174.
[25] T. Doshida and K. Takai, Dependence of hydrogen-induced lattice defects and hydrogen embrittlement of cold-drawn pearlitic steels on hydrogen trap state, temperature, strain rate and hydrogen content, *Acta Mater.*, 79(2014), p. 93.
[26] I. Moro, L. Briottet, P. Lemoine, E. Andrieu, C. Blanc, and G. Odemer, Hydrogen embrittlement susceptibility of a high strength steel X80, *Mater. Sci. Eng. A*, 527(2010), No. 27-28, p. 7252.
[27] X. Zhu, W. Li, H.S. Zhao, L. Wang, and X.J. Jin, Hydrogen trapping sites and hydrogen-induced cracking in high strength quenching & partitioning (Q&P) treated steel, *Int. J. Hydrogen Energy*, 39(2014), No. 24, p. 13031.
[28] S.J. Kim, D.W. Yun, H.G. Jung, and K.Y. Kim, Determination of hydrogen diffusion parameters of ferritic steel from electrochemical permeation measurement under tensile loads, *J. Electrochem. Soc.*, 161(2014), No. 12, p. E173.
[29] F. Huang, X.G. Li, J. Liu, Y.M. Qu, J. Jia, and C.W. Du, Hydrogen-induced cracking susceptibility and hydrogen trapping efficiency of different microstructure X80 pipeline steel, *J. Mater. Sci.*, 46(2011), No. 3, p. 715.
[30] M. Koyama, E. Akiyama, and K. Tsuzaki, Effect of hydrogen content on the embrittlement in a Fe–Mn–C twinning-induced plasticity steel, *Corros. Sci.*, 59(2012), p. 277.
[31] Y.X. Chen, S.Q. Zheng, J. Zhou, P.Y. Wang, L.Q. Chen, and Y.M. Qi, Influence of H_2S interaction with prestrain on the mechanical properties of high-strength X80 steel, *Int. J. Hydrogen Energy*, 41(2016), No. 24, p. 10412.
[32] P.C. Okonkwo, R.A. Shakoor, A. Soliman, and A.M.A. Mohammed, Corrosion behavior of API X-80 steel in hydrogen sulfide environment at different temperatures, [in] *Corrosion 2016*, Vancouver, 2016.
[33] K. Shen, L. Xu, Y. Guo, J. Shi, and M.Q. Wang, Effect of microstructure on hydrogen diffusion and notch tensile strength of large steel forging, *Mater. Sci. Eng. A*, 628(2015), p. 149.
[34] T. Michler, M. Lindner, U. Eberle, and J. Meusinger, Assessing hydrogen embrittlement in automotive hydrogen tanks, [in] R.P. Gangloff and B.P. Somerday eds. *Gaseous Hydrogen Embrittlement of Materials in Energy Technologies*, Woodhead Publishing, Cambridge, 2012, p. 94.
[35] T. Depover and K. Verbeken, The effect of TiC on the hydrogen induced ductility loss and trapping behavior of Fe–C–Ti alloys, *Corros. Sci.*, 112(2016), p. 308.
[36] Y.M. Qi, H.Y. Luo, S.Q. Zheng, C.F. Chen, and D.N. Wang, Effect of immersion time on the hydrogen content and tensile properties of A350LF2 steel exposed to hydrogen sulphide environments, *Corros. Sci.*, 69(2013), p. 164.
[37] J. Kittel, V. Smanio, M. Fregonese, L. Garnier, and X. Lefebvre, Hydrogen induced cracking (HIC) testing of low alloy steel in sour environment: Impact of time of exposure on the extent of damage, *Corros. Sci.*, 52(2010), No. 4, p. 1386.
[38] W.Y. Chu, L.J. Qiao, Y.B. Wang, and Y.H. Cheng, Quantitative study for sulfide stress corrosion cracking of tubular steel, *Corrosion*, 55(1999), No. 7, p. 667.
[39] G. Hultquist, M.J. Graham, J.L. Smialek, and B. Jönsson, Hydrogen in metals studied by thermal desorption spectroscopy (TDS), *Corros. Sci.*, 93(2015), p. 324.
[40] M. Kaneko, T. Doshida, and K. Takai, Changes in mechan-

ical properties following cyclic prestressing of martensitic steel containing vanadium carbide in presence of nondiffusible hydrogen, *Mater. Sci. Eng. A*, 674(2016), p. 375.

[41] D. Vo, A. Lipnitskii, T. Nguyen, and T.K. Nguyen, Nitrogen trapping ability of hydrogen-induced vacancy and the effect on the formation of AlN in aluminum, *Coatings*, 7(2017), No. 6, p. 79.

[42] H. Sugimoto and Y. Fukai, Hydrogen-induced superabundant vacancy formation by electrochemical methods in bcc Fe: Monte Carlo simulation, *Scripta Mater.*, 134(2017), p. 20.

[43] I.M. Robertson, P. Sofronis, A. Nagao, M.L. Martin, S. Wang, D.W. Gross, and K.E. Nygren, Hydrogen embrittlement understood, *Metall. Mater. Trans. A*, 46(2015), No. 6, p. 2323.

[44] Y. Tateyama and T. Ohno, Stability and clusterization of hydrogen-vacancy complexes in α-Fe: an ab initio study, *Phys. Rev. B*, 67(2003), No. 17, art. No. 174105.

[45] H.G.F. Wilsdorf, The ductile fracture of metals: a microstructural viewpoint, *Mater. Sci. Eng.*, 59(1983), No. 1, p. 1.

[46] H.G.F. Wilsdorf, The role of glide and twinning in the final separation of ruptured gold crystals, *Acta Metall.*, 30(1982), No. 6, p. 1247.